

Efficient 2.5D Hand Pose Estimation via Auxiliary Multi-Task Training for Embedded Devices

Prajwal Chidananda, Ayan Sinha, Adithya Rao, Douglas Lee, and Andrew Rabinovich
Magic Leap, Inc.

(pchidananda, asinha, arao, dlee, arabinovich) @magic Leap.com

Abstract

2D Key-point estimation is an important precursor to 3D pose estimation problems for human body and hands. In this work, we discuss the data, architecture, and training procedure necessary to deploy extremely efficient 2.5D hand pose estimation on embedded devices with highly constrained memory and compute envelope, such as AR/VR wearables. Our 2.5D hand pose estimation consists of 2D key-point estimation of joint positions on an egocentric image, captured by a depth sensor, and lifted to 2.5D using the corresponding depth values. Our contributions are two fold: (a) We discuss data labeling and augmentation strategies, the modules in the network architecture that collectively lead to 3% the flop count and 2% the number of parameters when compared to the state of the art MobileNetV2 [13] architecture. (b) We propose an auxiliary multi-task training strategy needed to compensate for the small capacity of the network while achieving comparable performance to MobileNetV2. Our 32-bit trained model has a memory footprint of less than 300 Kilobytes, operates at more than 50 Hz with less than 35 MFLOPs.

1. Introduction

Hand pose estimation is a critical component of mixed reality (MR) applications to enable controller-less interactions. It comes in different forms.

- Discrete pose classification: The objective is to classify the hand pose into one of predefined classes such as OK, thumbs up, open hand etc. [8]
- 2D hand key-point estimation: Here, a select number of key-points on the hand are detected in the image. These usually correspond to visible joint positions of the hand skeleton [14].
- 2.5D hand key-point estimation: Similar to 2D hand key-point estimation, select skeletal joint positions are

detected in the image. Additionally, the key-points are lifted to 2.5d using corresponding depth values of the estimated 2D joint pixels in the image.

- 3D hand key-point estimation: All key-points corresponding to skeletal joint positions are detected in 3D coordinates. The 3D detection corresponds to plausible anthropomorphic configurations of the human hand [9, 10].
- Fully articulated 3D hand: The full mesh of the hand is detected and tracked. This corresponds to 3D hand key-point estimation in conjunction with 3D hand shape estimation [12, 17].

In this article we focus on 2.5D hand key-point estimation. While such an approach suffices for most hand interactions in AR/VR/MR environments, it fails when the key-points on the hand are self-occluded and the depth corresponds to hand surface's depth ignoring occlusions.

2. Data, labeling, and augmentation

The input to the vision-based hand tracking systems is often either a monocular rgb/grayscale image or a depth image. Depth-based approaches have been shown to outperform RGB-based approaches for 3D pose estimation [1, 4, 3, 11, 19, 15]. For our implementation, we use a time-of-flight (TOF) depth sensor.

Using mechanical turk, we labeled 17 key-points per image. The labelers only label the visible key-points which correspond to all. Although the network only predicts 8 key-points, the additional key points serve as auxiliary supervision (described in section 4). Images of hands are also labeled with 8 discrete hand key-pose classes, as well as right/left hand assignments. Later, we describe how additional labels act as supervisory tasks.

To avoid hand-like (distractor) objects confounding the predictions, we composite the images containing the hand with varied backgrounds containing challenging distractor objects. By collecting data in controlled environments and

using augmentation, we expand the training data to generalize to different environments. As most of the collected data is for a user performing single handed interactions, a skew is introduced in the dataset. To mitigate this, left and right hands are composited from different images to look like two handed interactions.

3. Network Modeling

TOF depth sensors capture phase images which are then translated to a depth image using post-processing. The compute time for post-processing the phase images to calculate the depth image adds a considerable portion to the end-to-end latency for hand tracking. Towards addressing this issue, we explore directly using a linear combination of phase images, which we term *amplitude* image to perform 2D key-point estimation and perform depth image processing in parallel, this effectively reducing the overall latency. As discussed later, this improves performance while removing around 20ms latency of the sequential depth processing by doing it in parallel.

Our network follows an encoder-decoder structure. The encoder is organized as a pipeline of tiers; where each tier is a concatenation of units and each unit is a combination of blocks as shown in Fig. 1. We use a variant of the DenseNet [6] block in Tier-2, wherein we use two Conv-BN-ReLU model blocks instead of the conventional four blocks in order to reduce sequential compute. Unlike in DenseNet, we do not concatenate the input tensor with the intermediate feature tensors. This reduces compute and stems from our observation that the input feature tensor is mostly redundant and does not contribute to performance gains. However, removing the input tensor slows down training. Hence, in Tier-3 we replace the standard Conv-BN-ReLU model blocks with ResNet blocks to improve information flow during back-propagation. Furthermore, we use a ladder of bottleneck ResNet blocks wherein each module has convolution with a different dilation rate, i.e., 4 bottleneck ResNet blocks with a dilation rate of 1,2,3,4 respectively. Overall, our network combines the best of DenseNet’s feature reuse property and ResNet’s [5] information flow property.

We also use small number of channels to reduce parallel compute with 16 channels after Tier-1, 32 channels after Tier-2, and 64 channels after Tier-3. Furthermore, we use dilated convolutions in Tier-3 to increase the receptive field of our relatively shallow network.

We employ grouped convolutions at all but first tier so as to reduce compute. In Tier-2 we use grouping factor of 4 and we use grouping factor of 8 in Tier-3. In our experiments, we observed that the encoder is responsible for a majority of the gains in performance, and changing the decoder architecture only marginally affects performance. Hence, our key-point decoder is very lean and all convolutions are channel wise, i.e., number of groups is equal to the

number of channels.

Embedded Implementation

The embedded implementation of our network architecture is carefully designed to reduce compute / memory overhead and energy consumption. The Myriad2 VPU runs at 600MHz and provides 12 VLIW compute cores called SHVs. Under typical workloads, total power consumption of the Myriad2 chip is less than 2W. Each SHV is allocated a 128KB working memory slice out of 2MB on-chip SRAM. Our Gestures DNN must perform real-time 45FPS hand tracking and gesture recognition using a single SHV.

Using conventional implementations makes these minimization challenging for several reasons: (a) Typical deep learning frameworks convert convolution into a large matrix multiply in a highly memory inefficient way (b) Input data tensors are typically stored in channel planar format, which is inefficient for vectorization. (c) The kernel sizes are often not a multiple of the vector instruction width (d) Off-the-shelf implementations of dilated convolutions have considerable computational overhead.

To address these challenges, (a) We reorder and interleave the input data channels to each convolution layer to align with vector instruction ordering. We simultaneously reorder the kernel stack such that convolutions are reduced to dot products and the output channel is automatically encoded in the interleaved format for the next layer. (b) We group convolution layers so that the number of filters per group is a multiple of the register lanes, consequently, maximizing vector register utilization. (c) We use a comb design for dilated convolutions which minimizes the on-chip memory footprint. For example, for dilation=2, convolution splits into four independent field-wise computations (even rows-even columns, even-odd, etc) which are computed independently and recombined on output. Dilated convolutions are thus computed at zero effective overhead.

4. Training

We adopt a multi-task learning paradigm in the training procedure by employing multiple network predictions and loss functions, while maintaining the the prime focus on 2D key-point prediction. Note that human labeling for auxiliary tasks such as discrete hand pose or categorical orientation is much faster than key-point labeling, or comes for free with key-point labeling such as key-point visibility. At inference time, only the primary encoder and decoder are part of the network running on device.

Cross entropy with 1-hot label is used to predict each of the 16 key-points (8 key-points per hand). We observed that the aggressive down-sampling in the early layers coupled with the low network capacity, makes the conventional mean squared loss (MSE) loss ineffective. Cross entropy has a stronger gradient signal and is much more effective.

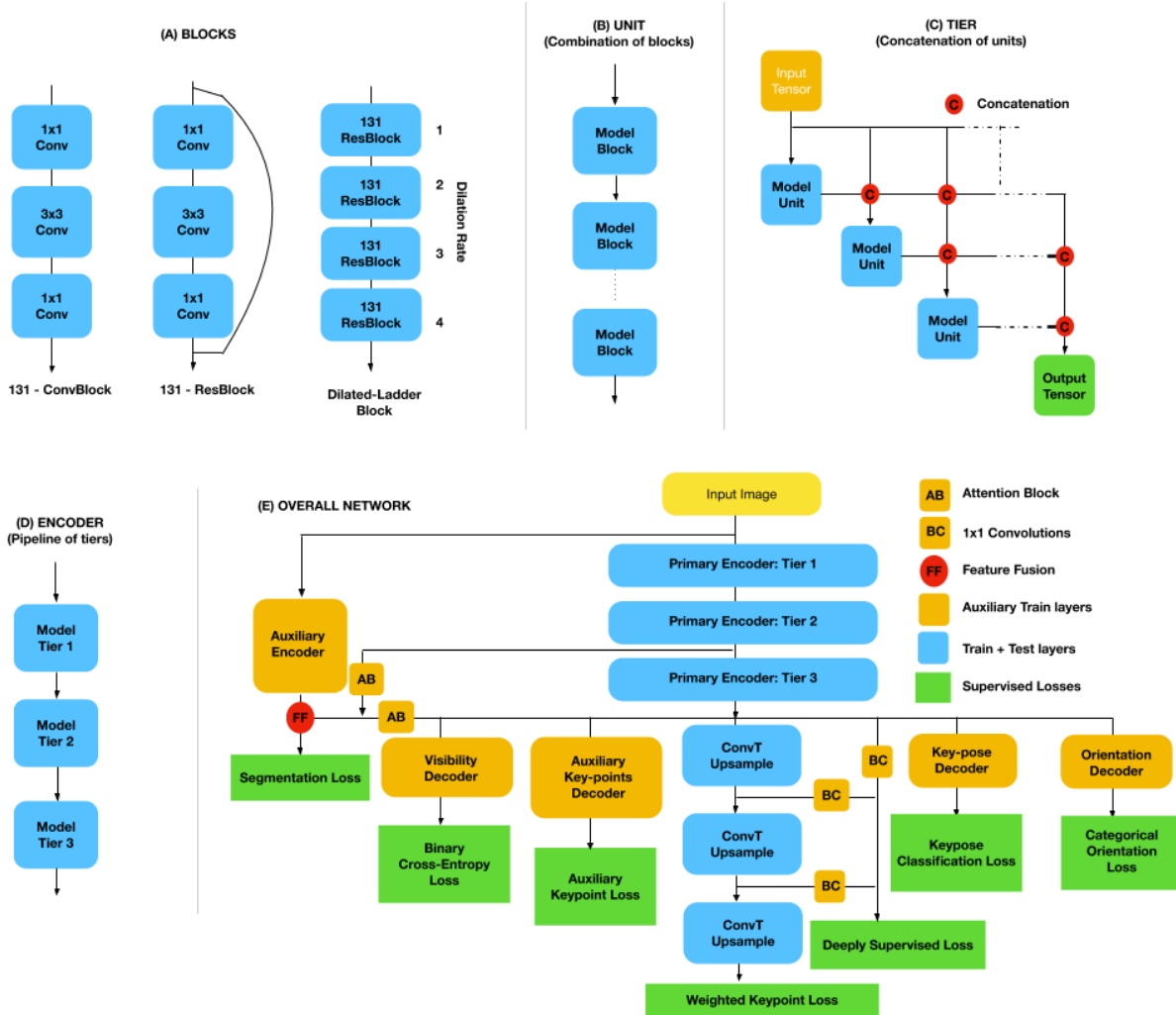


Figure 1. (A) Model Blocks used in our network architecture (B) Model Units: a combination of model blocks, (C) Model Tier: a concatenation of model units, which could be seen as a variant of the DenseBlock, (D) Primary encoder: a pipeline of three tiers, (E) Overall network architecture along with auxiliary modules with corresponding supervised losses trained end-to-end for our 2.5D hand key-point estimation. Our Tier-1 is a simple convolution layer, Tier-2 is composed of two 131-ConvBlocks, and Tier-3 is composed of two Dilated-Ladder units.

We experimented with label smoothing but did not observe performance gains.

Given that we have 17 key-point labels per hand, we use the additional key-points as training supervision, even though they are not part of the final inference module. As our decoder is composed of fully grouped convolutions, we observed some key-points failing to train all together. Hence, the decoder for the auxiliary key-points do not use grouping in the convolutions so as to avoid floating key-points and regularize the feature tensor after the encoder.

The binary key-point and hand visibility masks serve three purposes: make training stable, suppress occluded

key-points and invisible hands during inference, enable an early out during inference to reduce latency. We use a binary cross entropy loss to train these tasks.

The data collected was heavily skewed against palm-facing data causing the trained model to under-perform on palm-facing data. To address this, we regularized the predictions using a categorical hand orientation loss. We label 8 categorical hand orientations that could arise from supination or pronation of the hand. Since the categories are approximate, we soften the labels and use cross-entropy loss to train these tasks.

We classify the hand pose into nine discrete classes: OK,

open-hand, pinch, C-pose, fist, L-pose, point, thumbs-up, and a dummy class capturing all other poses. We use cross-entropy loss to train the discrete hand-pose classification.

Following the architecture of BiSeNet proposed [18], we use our network architecture discussed previously as the context path and use a spatial path similar to BiSeNet as a training-time artifact to provide useful supervision that regularizes the key-points that jump off the hand. We train the network to segment three classes: background, left hand and right hand using a per-pixel cross entropy loss.

We observe that key-points often fail to train due to the grouped structure of decoder. Following [16], we add additional key-point supervision heads after three intermediate layers, with different spatial resolutions: tier 3 of the primary encoder (1/8th the full resolution), the first up-sampling block (1/4th the full resolution) and the second up-sampling block (1/2 the full resolution). This stabilizes training and facilitates better gradient flow for training.

Our final loss is a weighted sum of all the individual task losses: primary key-point loss \mathcal{L}_{kp} , auxiliary key-point loss \mathcal{L}_{akp} , key-point and hand visibility loss \mathcal{L}_{kphv} , categorical hand orientation loss \mathcal{L}_{cho} , discrete hand pose loss \mathcal{L}_{dhp} , segmentation loss \mathcal{L}_{seg} , deep supervision loss \mathcal{L}_{ds} .

We use task-weighting to weigh the different losses, as the predictions are not all at the same scale. The weights for the different tasks were derived heuristically, but can be replaced with an adaptive weighting using gradient normalization as described in [2]. The full training loss with all task losses and corresponding weights are shown in Eq 1.

$$\mathcal{L}_{total} = w_{kp}\mathcal{L}_{kp} + w_{akp}\mathcal{L}_{akp} + w_{kphv}\mathcal{L}_{kphv} + w_{cho}\mathcal{L}_{cho} + w_{dhp}\mathcal{L}_{dhp} + w_{seg}\mathcal{L}_{seg} + w_{ds}\mathcal{L}_{ds} \quad (1)$$

where $w_{kp} = 1$, $w_{akp} = 1$, $w_{kphv} = 20$, $w_{cho} = 20$, $w_{dhp} = 10$, $w_{seg} = 50$, $w_{ds} = 1$.

We empirically observe that the network finds it harder to predict finger tips when compared to the other key-points. We address this by simply doubling the losses for finger tips while calculating \mathcal{L}_{kp} and \mathcal{L}_{akp} .

Table 1. Ablation study: Each supervision technique is removed and the corresponding average key-point errors are shown. \mathcal{W}_k here represents key-point loss weighting.

Input mode	\mathcal{L}_{seg}	\mathcal{L}_{ds}	\mathcal{L}_{cho}	\mathcal{W}_k	\mathcal{L}_{kphv}	\mathcal{L}_{dhp}	Err (px)
Depth	×	×	×	×	×	×	6.226
Amplitude	×	×	×	×	×	×	6.054
Amplitude	✓	✓	×	✓	✓	✓	5.941
Amplitude	✓	✓	✓	×	✓	✓	5.730
Amplitude	✓	×	✓	✓	✓	✓	5.994
Amplitude	×	✓	✓	✓	✓	✓	5.690
Amplitude	✓	✓	✓	✓	✓	×	5.655
Depth	✓	✓	✓	✓	✓	✓	5.898
Amplitude	✓	✓	✓	✓	✓	✓	5.556

Table 2. Comparison of size, computational cost and performance between DenseNet, MobileNet-V2 and Our implementation.

Backbone	Parameters	GFLOPs	Keypoint Error
DenseNet	7.017M	4.866	4.457px
MobileNetV2	1.893M	1.209	5.306 px
Ours	0.041M	0.035	5.556 px

Table 3. Comparison of inference time for a single forward pass on an Intel Movidius Myriad between mvTensor and our custom implementation.

Shave #	1	2	3	4	6
mvTensor (ms)	205.0	114.0	84.0	68.0	54.0
Ours (ms)	16.0	-	-	-	-

5. Results and Discussion

We evaluate our method on its 2D key-point estimation performance and run time performance on an Intel Movidius Myriad chip, which affects latency. We run experiments on a reduced in-house dataset that has 40 users using a train/validation/test split of 28/4/8. The dataset has over 5K frames per user, with a total 225733 frames. To quantitatively evaluate the key-point estimation, we report the average 2D euclidean distance between the estimated 2D key-points and the ground truth, expressed in pixels.

First, we evaluate the impact of all the losses used in the training scheme by doing an ablation study. The models are all trained for 20 epochs, with a learning rate of 0.001 with a linear decay, using Adam as the optimizer. As shown in Table 1, each loss positively contributed to the performance and the model which has all the training losses performs best. Furthermore, the amplitude image as input to the network consistently performs better than the depth image input, while also reducing latency. Note, at run-time we lift the 2D predictions on amplitude image to 2.5D using the depth image processed in parallel. We use simple filtering and heuristics to ensure valid depth for identified 2D key-points.

Second, we compare our model with DenseNet-121 [6] and MobileNet-V2 [13] in terms of the number of model parameters, the total number of floating point operations for a single frame, and the 2D key-point error. We use the same decoder for all three networks, with the same training scheme used in the ablation study. Table 2 compares the three models. We see that our model is 2% the size of MobileNetV2 in terms of parameters and has 3% the compute of MobileNetV2, with only 4.7% degradation in key-point localization performance.

We evaluate the run time performance of our implementation by comparing its latency with that of the off-the-shelf mvTensor implementation on the Intel Movidius Myriad [7]. Table 3 compares the two implementations. By re-

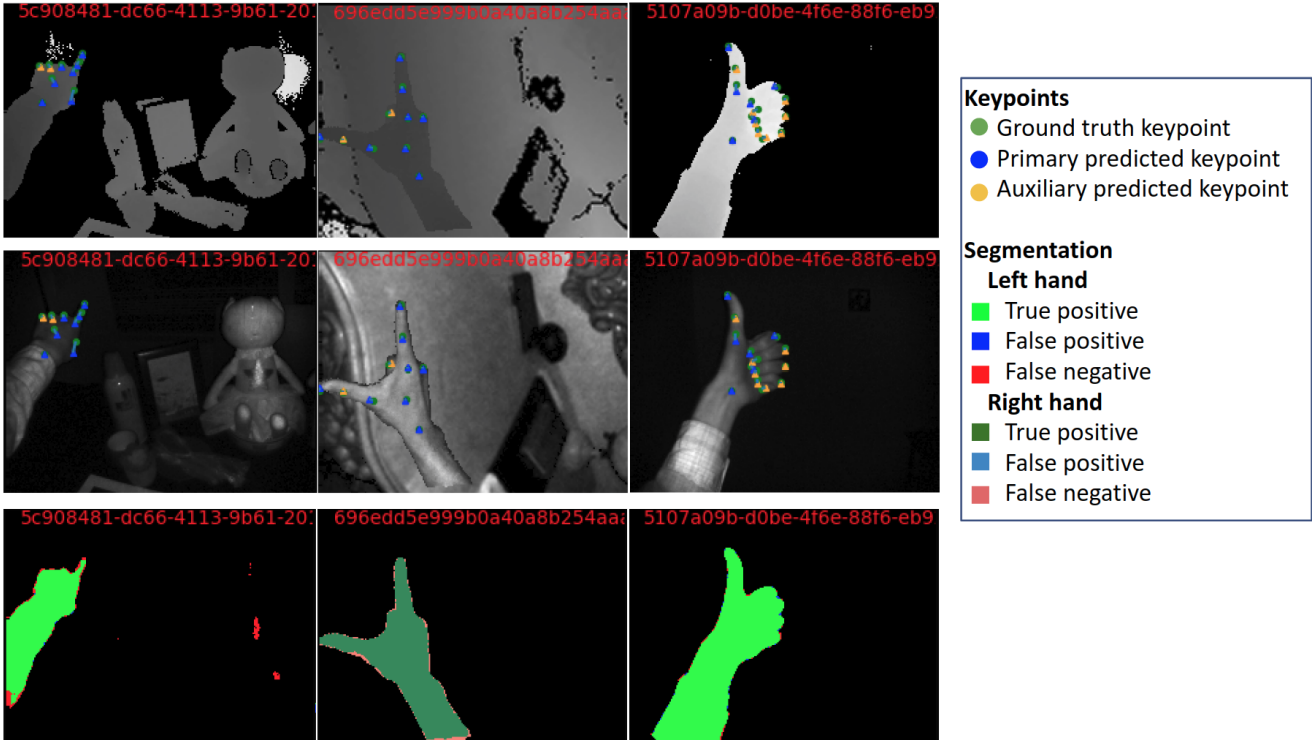


Figure 2. Qualitative results on our in-house dataset. Top row shows 2D key point predictions on depth images, Middle row shows 2D key point predictions on amplitude images, Bottom row shows corresponding segmentation results.

ordering of input activation channels and the kernel stack, having grouped convolution layers with a multiple-of-the-register-length number of kernels per group, and using an efficient comb design for dilation, our embedded implementation achieves 16ms latency, which is a 12x speedup over mvTensor.

Overall, we describe an end-to-end 2.5D key-point estimation system with unique insights at each stage of the pipeline: data, network architecture, training and embedded implementation. The first take-away is that auxiliary labeling and multi-task training is a viable strategy to improve performance of extremely compact network architectures bound by compute constraints on edge devices. Second, network architectures crafted in sync with embedded hardware operating constraints can offer significant benefits at run-time, vital for latency critical applications like hand-tracking.

6. Acknowledgements

We would like to acknowledge Lexin Tang at Magic Leap, Inc. for her work on the embedded code implementation.

References

- [1] Seungryul Baek, Kwang In Kim, and Tae-Kyun Kim. Augmented skeleton space transfer for depth-based hand pose estimation. In *Proceedings of the IEEE Conference on Computer Vision and Pattern Recognition*, pages 8330–8339, 2018. 1
- [2] Zhao Chen, Vijay Badrinarayanan, Chen-Yu Lee, and Andrew Rabinovich. Gradnorm: Gradient normalization for adaptive loss balancing in deep multitask networks. *arXiv preprint arXiv:1711.02257*, 2017. 4
- [3] Chiho Choi, Sang Ho Yoon, Chin-Ning Chen, and Karthik Ramani. Robust hand pose estimation during the interaction with an unknown object. In *Proceedings of the IEEE International Conference on Computer Vision*, pages 3123–3132, 2017. 1
- [4] Chiho Choi, Sangpil Kim, and Karthik Ramani. Learning hand articulations by hallucinating heat distribution. In *Proceedings of the IEEE International Conference on Computer Vision*, pages 3104–3113, 2017. 1
- [5] Kaiming He, Xiangyu Zhang, Shaoqing Ren, and Jian Sun. Deep residual learning for image recognition. In *Proceedings of the IEEE conference on computer vision and pattern recognition*, pages 770–778, 2016. 2
- [6] Gao Huang, Zhuang Liu, Laurens Van Der Maaten, and Kilian Q Weinberger. Densely connected convolutional networks. In *Proceedings of the IEEE conference on computer vision and pattern recognition*, pages 4700–4708, 2017. 2, 4

- [7] Mircea Horea Ionica and David Gregg. The movidius myriad architecture’s potential for scientific computing. *IEEE Micro*, 35(1):6–14, 2015. 5
- [8] Jason Isaacs and Simon Foo. Hand pose estimation for american sign language recognition. In *Thirty-Sixth Southeastern Symposium on System Theory, 2004. Proceedings of the*, pages 132–136. IEEE, 2004. 1
- [9] Gyeongsik Moon, Ju Yong Chang, and Kyoung Mu Lee. V2v-posenet: Voxel-to-voxel prediction network for accurate 3d hand and human pose estimation from a single depth map. In *Proceedings of the IEEE Conference on Computer Vision and Pattern Recognition*, pages 5079–5088, 2018. 1
- [10] Franziska Mueller, Florian Bernard, Oleksandr Sotnychenko, Dushyant Mehta, Srinath Sridhar, Dan Casas, and Christian Theobalt. Gnerated hands for real-time 3d hand tracking from monocular rgb. In *Proceedings of the IEEE Conference on Computer Vision and Pattern Recognition*, pages 49–59, 2018. 1
- [11] Franziska Mueller, Dushyant Mehta, Oleksandr Sotnychenko, Srinath Sridhar, Dan Casas, and Christian Theobalt. Real-time hand tracking under occlusion from an egocentric rgb-d sensor. In *Proceedings of the IEEE International Conference on Computer Vision*, pages 1284–1293, 2017. 1
- [12] Georgios Pavlakos, Vasileios Choutas, Nima Ghorbani, Timo Bolkart, Ahmed AA Osman, Dimitrios Tzionas, and Michael J Black. Expressive body capture: 3d hands, face, and body from a single image. *arXiv preprint arXiv:1904.05866*, 2019. 1
- [13] Mark Sandler, Andrew Howard, Menglong Zhu, Andrey Zhmoginov, and Liang-Chieh Chen. Mobilenetv2: Inverted residuals and linear bottlenecks. In *Proceedings of the IEEE Conference on Computer Vision and Pattern Recognition*, pages 4510–4520, 2018. 1, 4
- [14] Tomas Simon, Hanbyul Joo, Iain Matthews, and Yaser Sheikh. Hand keypoint detection in single images using multiview bootstrapping. In *Proceedings of the IEEE Conference on Computer Vision and Pattern Recognition*, pages 1145–1153, 2017. 1
- [15] Ayan Sinha, Chiho Choi, and Karthik Ramani. Deephand: Robust hand pose estimation by completing a matrix imputed with deep features. In *Proceedings of the IEEE conference on computer vision and pattern recognition*, pages 4150–4158, 2016. 1
- [16] Liwei Wang, Chen-Yu Lee, Zhuowen Tu, and Svetlana Lazebnik. Training deeper convolutional networks with deep supervision. *arXiv preprint arXiv:1505.02496*, 2015. 4
- [17] Donglai Xiang, Hanbyul Joo, and Yaser Sheikh. Monocular total capture: Posing face, body, and hands in the wild. *arXiv preprint arXiv:1812.01598*, 2018. 1
- [18] Changqian Yu, Jingbo Wang, Chao Peng, Changxin Gao, Gang Yu, and Nong Sang. Bisenet: Bilateral segmentation network for real-time semantic segmentation. In *Proceedings of the European Conference on Computer Vision (ECCV)*, pages 325–341, 2018. 4
- [19] Shanxin Yuan, Guillermo Garcia-Hernando, Björn Stenger, Gyeongsik Moon, Ju Yong Chang, Kyoung Mu Lee, Pavlo Molchanov, Jan Kautz, Sina Honari, Liuhao Ge, et al. Depth-based 3d hand pose estimation: From current achievements to future goals. In *Proceedings of the IEEE Conference on Computer Vision and Pattern Recognition*, pages 2636–2645, 2018. 1